energies

MDPI

Article

The Effects of γ-Radiation on the Physical and Electrical Properties of Silicone Encapsulation for Electronic Power Conditioners

Cong Hu [1,2,*], Wei Zheng [1,2], Bin Zhao [1], Yu Fan [1], Hong Li [1], Kun Zheng [3] and Gang Wang [1,2,*]

[1] Aerospace Information Research Institute, Chinese Academy of Sciences, Beijing 100094, China
[2] School of Electronic, Electrical and Communication Engineering, University of Chinese Academy of Sciences, Beijing 100049, China
[3] Key Laboratory of Science and Technology on High-Tech Polymer Materials, Chinese Academy of Sciences, Beijing 100190, China
* Correspondence: hucong@aircas.ac.cn (C.H.); wanggang002412@aircas.ac.cn (G.W.); Tel.: +86-135-8168-5224 (C.H.)

Abstract: Since the electronic power conditioner (EPC) is a crucial part of a space traveling-wave tube amplifier (STWTA), its reliability issue must be considered. The most effective way to prevent insulation breakdown is potting. Silicone elastomers are commonly used as an encapsulant for the EPC because of their good physical and electrical properties. The properties of the encapsulant and the interfaces change under the influence of γ-radiation, which may result in the failure of the potted modules. In this work, a comprehensive evaluation methodology is proposed for silicone-based potted modules, where besides physical and electrical properties, the effect of γ-radiation on the encapsulated interface is also considered. The results show that with the increase of the irradiation dose, the crosslinking density, hardness, elastic modulus, volume resistivity, dielectric constant, and storage modulus are increased by 301.6%, 76.3%, 289.7%, 396.1%, 5.0%, and 589.8%, respectively. In contrast, the elongation at break and dielectric loss factor are decreased by 83.8% and 57.8%. In addition, the tensile strength and breakdown strength first increase and then decrease, while the coefficient of thermal expansion of the interface shows the opposite trend. Since the interface bonding state does not change and the electric field strength of the tip decreases slightly with an increasing dielectric constant, the average value of the partial discharge inception voltage increased slightly.

Keywords: space traveling-wave tube amplifier; electronic power conditioner; silicone encapsulation; γ-radiation; interface discharge; interface bonding

Citation: Hu, C.; Zheng, W.; Zhao, B.; Fan, Y.; Li, H.; Zheng, K.; Wang, G. The Effects of γ-Radiation on the Physical and Electrical Properties of Silicone Encapsulation for Electronic Power Conditioners. *Energies* **2023**, *16*, 2028. https://doi.org/10.3390/en16042028

Academic Editor: Abu-Siada Ahmed

Received: 22 January 2023
Revised: 5 February 2023
Accepted: 16 February 2023
Published: 18 February 2023

1. Introduction

The space traveling-wave tube amplifier (STWTA) is a key component of satellite systems for satellite communication and spaceborne transponders. It is mainly responsible for the amplification, forwarding, and transmission of microwave signals [1]. The most effective way to prevent insulation breakdown of the electronic power conditioner (EPC), which is a critical component of STWTA [2], is potting [3]. The EPC contains a variety of components in different types and packages, and the coefficient of thermal expansion (CTE) varies substantially between different materials. Silicone elastomers are the most commonly used encapsulants for the EPC due to their unique performance and low stress concentration [4]. In addition to being influenced by temperature, the potted modules of EPCs used in complex space environments are also exposed to radiation from various particles [5,6]. The radiated energy can reach a few MeV. On the other hand, the dissociation energy of the chemical bonds of silicone elastomers is only 2–4 eV, and the ionization energy is only 9–15 eV. The radiated energy far exceeds the dissociation energy or ionization energy of the chemical bonds, inducing a radiation chemical effect on the silicone elastomer, which results

in the degradation of its material properties [7]. Researchers have carried out a series of studies on the irradiation aging of silicone elastomers [8,9]. Studies on different irradiation types have shown that the irradiation aging of silicone elastomers mainly depends on the total irradiation dose, regardless of the irradiation type [9,10]. Research on silicone elastomers used in nuclear power plants has mainly focused on the change in the mechanical properties in the combined aging due to γ-radiation and heat [11–13]. Investigations have been carried out to study the γ-radiation-induced degradation of the mechanical and electrical properties of silicone elastomers used as composite insulators [14–17]. It is of interest to study the effects of radiation on the thermal behavior of silicone elastomers through dynamic mechanical analysis (DMA) as a means to investigate the radiation-induced degradation of polymer insulating materials [18]. Researchers have also studied the effect of γ-radiation on the silicone encapsulant and binder [19–21].

However, it is worth noting that previous studies focused on the effects of irradiation on the mechanical and electrical properties of materials themselves, and the effect of irradiation on the encapsulated interface is rarely reported. In the EPC, the silicone encapsulant is used for the potting of high-voltage printed circuit boards, which exhibit a high electric field intensity, a complex internal structure, and an inhomogeneous electric field distribution [3]. Potting defects mainly occur in two forms: firstly, interface discharge, and interface debonding and delamination cause interface discharge [22–27]; secondly, the cracking of components and the fracture of solder joints caused by the increase in the local internal stress in the material [28,29], the generation of which is usually affected by the thermal expansion deformation of the interface [3,7]. As a result, in order to master the effect of irradiation on the potted module based on silicone encapsulant, it is necessary to design a comprehensive evaluation method, where besides physical and electrical properties, the effect of radiation on the encapsulated interface is also considered. In this work, the needle-plate electrodes were prepared as the interface partial discharge (PD) sample [30], and DMA and TMA were used to analyze the thermal behavior of the encapsulant [31]. The effects of γ-radiation on the physical, electrical, and interface properties of the silicone encapsulant and encapsulated interface samples were studied. Furthermore, the effect of irradiation on the properties of the encapsulant and the correlation between interfacial discharge and material properties and interfacial state were explored.

2. Materials and Methods

2.1. Experiment Design

^{60}Co γ-radiation was chosen as the irradiation source because ^{60}Co, being an artificial radionuclide, is currently the most commonly used source of γ-ray radiation. Furthermore, the cobalt source has the advantage of being characterized by a large irradiation space, and a large sample can be deposited in the same batch of the test. The total radiation doses were 10^5, 2.5×10^7, and 5×10^7 rad (Si), with a radiation dose rate of 50 rad (Si)/s. This total dose refers to the radiation to which the STWTA is subjected in different orbits. The silicone encapsulant and encapsulated interface were selected as the test objects. Figure 1 shows the evaluation method of a potting module. The main items of the evaluation are the physical and electrical properties of the encapsulant, as well as the encapsulated interface properties. The physical properties include mechanical properties and thermal behavior. The thermal behavior was studied mainly to analyze the evolution of the storage modulus and thermal deformation of the material with temperature, which can provide reference data for stress analysis based on finite element analysis. The interfacial properties include interfacial PD, interfacial bond, and interfacial expansion deformation. In addition, infrared analysis and microscopic morphology observations of the encapsulant were performed.

The infrared spectra of silicone encapsulant before and after irradiation were obtained via Fourier transform infrared spectroscopy (FTIR)-WQF-530K produced by Beijing Beifen-Ruili Analytical Instrument (Group) Co., Ltd. (Beijing, China).

Scanning electron microscope (SEM) (JSM-6510) of JEOL was used to observe the microscopic morphology of the samples before and after irradiation.

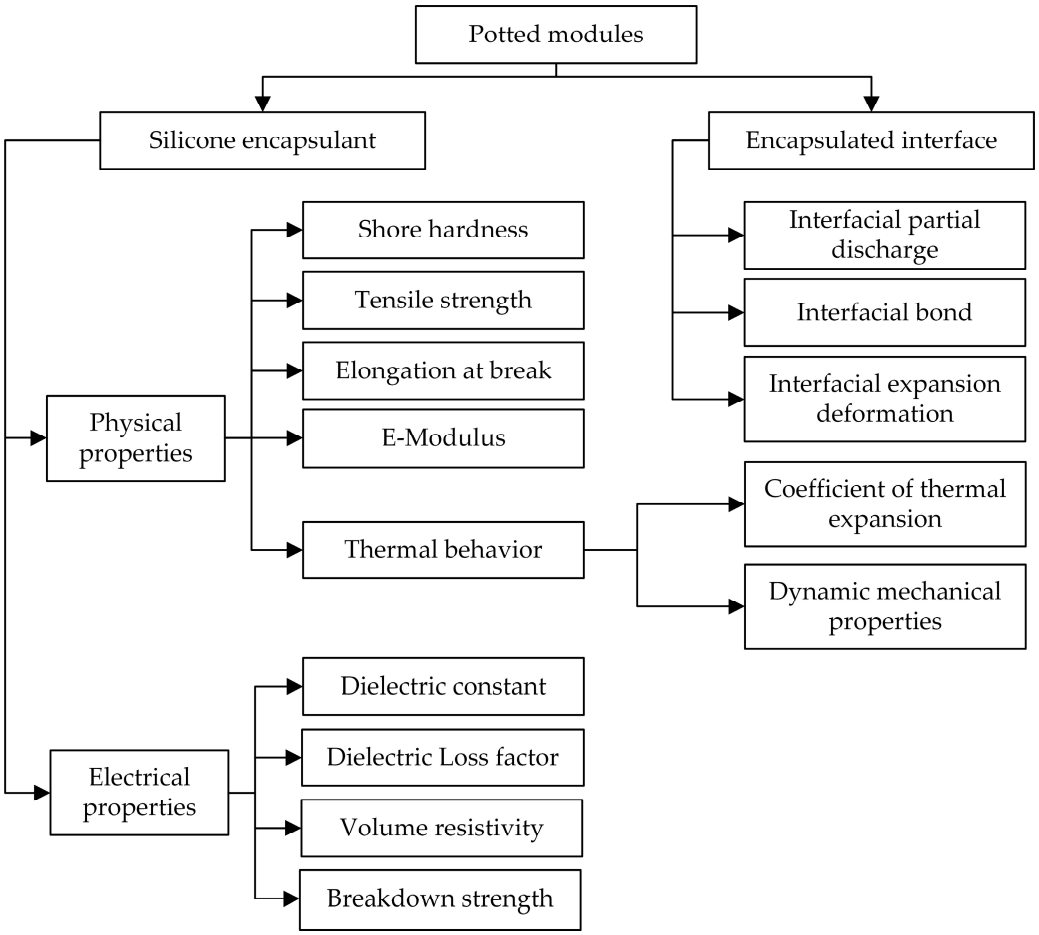

Figure 1. Test projects.

2.2. Test Sample Preparation

2.2.1. Silicone Encapsulant

The encapsulant used in the test was a silicone encapsulant for the EPC. The silicone encapsulant was potted into several samples with thicknesses of 1 and 2 mm in special molds. The samples were cut into dimensions and quantities corresponding to the test items before and after being subjected to γ-radiation. The size of the hardness test sample was ø30 × 6 mm.

2.2.2. Encapsulated Interface Discharge Sample

The internal circuit structure of the EPC is complex, as it exhibits an inhomogeneous field distribution, which may lead to PD. Internal electric field simulations show that the field strength is the highest at the interface between the silicone encapsulant and the internal structure [22].

The main interface involved in the potted modules of the EPC is the interface between the potting material and FR-4. To simulate an inhomogeneous field distribution, a needle-plate electrode was designed. The substrate consisted of an FR-4 plate with a thickness of 2 mm, a copper layer with a thickness of 38 μm, and a tip with a curvature radius of 10 μm. High-voltage wires were welded at the corresponding positions of the needle electrode and the plate electrode, and the solder joints were rounded. After cleaning, a void-free encapsulation technique was employed to ensure that there were no bubbles in the samples. Figure 2 shows a schematic diagram of the interface discharge sample.

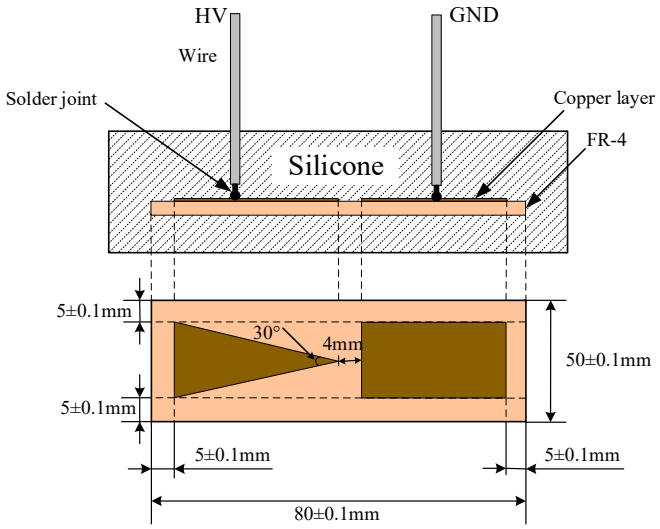

Figure 2. Encapsulation interface.

2.2.3. Interface Bonding Sample

The bonding interface was made with a 90° peel strength sample following the ISO 813:2019 standard. Figure 3 shows the actual and dimensional drawings of the peeled specimen.

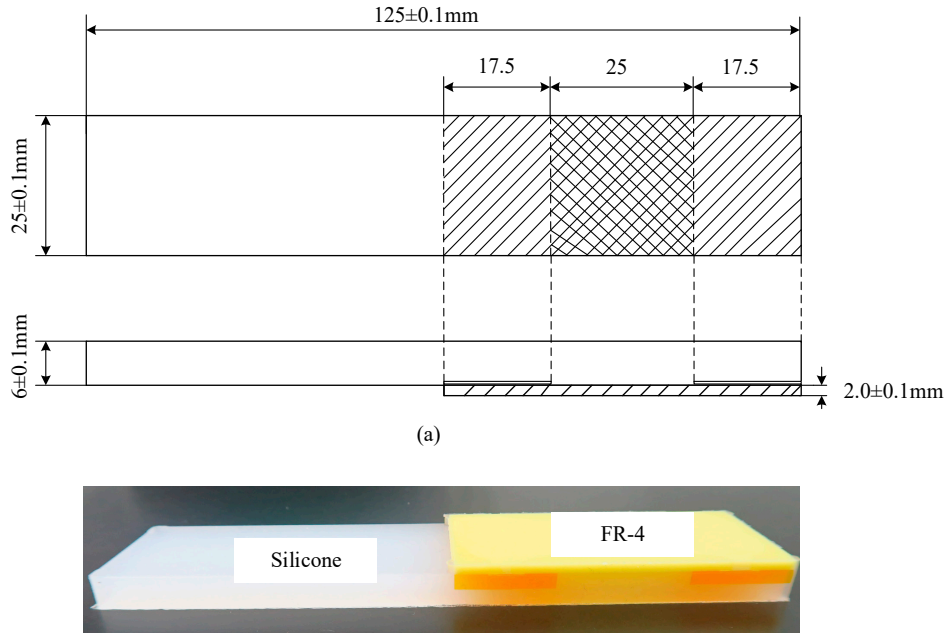

Figure 3. Interface bonding sample, (**a**) dimensional drawings of the peeled sample, (**b**) sample of interface bonding.

2.3. PD Inception Voltage Test

Figure 4 shows the schematic diagram of the PD test system, which was designed by the Aerospace Information Research Institute for PD detection of EPC components with a high sensitivity and a low discharge magnitude. In this work, the system was used to test the PD (PD) inception voltage of the needle-plate electrode potting samples under different irradiation conditions. The test method was based on reference [32], except for the fact that we prepared 10 samples for each group test.

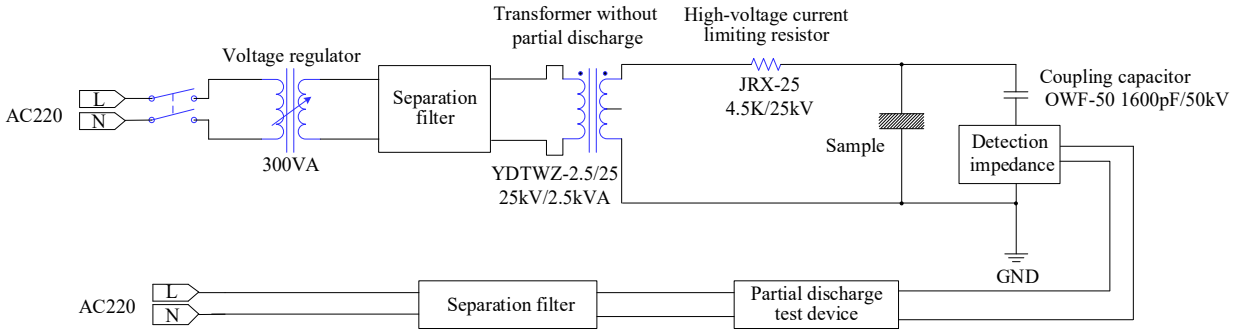

Figure 4. PD test system.

2.4. 90° Peel Test

A universal material testing machine was used to carry out the 90° peel test. Five samples were tested for each condition, and the average peel strength was taken. To further explore the interfacial bonding mechanism, the solvent erosion analysis method was used. An ammonia-saturated toluene solution was prepared by injecting 100 mL of ammonia and 300 mL of toluene into a 500 mL jar, shaking the obtained solution for around 5 min, and letting it rest for around 2 h. The silicone-encapsulated/FR-4 bonded samples under different irradiation conditions were immersed in the above toluene solution for 12 h, and the erosion of the bonding interface of the samples was evaluated. Similarly, the samples were immersed in toluene for 12 h to observe the erosion caused by the toluene solvent on the bonding interface of the specimens. According to Polmanteer's theory [33], it was judged that the bond was either a dispersion bond, a hydrogen bond, or a chemical bond.

2.5. Physical Property Tests

All tests of the physical properties were carried out under standard laboratory conditions. The samples were prepared and tested following the relevant standards. The samples for the physical property tests as well as the standards, test conditions, and test equipment are shown in Table 1.

Table 1. Samples for the physical property tests, standards, test conditions and test equipment.

Performances		**Standard**	**Test Equipment**	**Test Conditions**
Shore hardness		IEC 62217:2005	Shore A hardness tester	Sample: ø30 × 6 mm; Number of samples: 3
Tensile strength Elongation at break E-Modulus		ISO 37:2005	Universal material testing machine	Sample: dumbbell specimens with a length of 75 mm; Number of samples: 5
Thermal behavior	Dynamic mechanical properties	Instruction book	Mettler Toledo DMA-1	Sample: 10 mm × 6 mm × 2 mm; Temperature range: −35~125 °C; Heating rate: 3 °C min^{-1}; Frequency: 1 Hz; Mode: tension
	Linear coefficient of thermal expansion	ASTM E831-13	NETZSCH TMA-402F3	Material sample: ø6 mm × 2 mm; Interfacial sample:25 × 6 × 8 mm Temperature range: −35~125 °C; Heating rate: 10 °C min^{-1}

2.6. Electrical Property Tests

All tests of the electrical properties were carried out under standard laboratory conditions. The samples were prepared and tested following the relevant standards. The samples for the electrical property tests as well as the standards, test conditions, and test equipment are shown in Table 2.

Table 2. Samples for the electrical property tests, standards, test conditions and test equipment.

Performances	Standard	Test Equipment	Test Conditions
Dielectric constant	ASTM D 150:1998	Keysight-E4980A MICROTEST-FX-0000C7	Electrode: ø38 mm; Voltage: 1 V; Frequency: 1 kHz, 100 kHz, 500 kHz,1 MHz; Sample: ø50 mm × 1 mm Number of samples: 6
Volume resistivity	IEC 60093:1993	Keysight-B2985A-16008B	Main electrode: ø50 mm; Voltage: 1 kV; Time: 60 s; Sample: 100 mm × 100 mm × 1 mm; Number of samples: 5
AC breakdown strength	IEC 60243-1:2013	HV-HIPOT-GDSA-80	Equal-diameter electrodes: ø25 mm; Rate of voltage rise: 500 V/s; Sample: ø50 mm × 1 mm; Number of samples: 10

2.7. Crosslinking Density Test

The crosslinking density was tested using a solvent swelling method. The silicone-encapsulated samples with a mass m_1 were placed into an Erlenmeyer flask. Around 30 mL of toluene was poured into it, and the flask was then sealed and stored in a constant-temperature water bath at 25 °C for 7 days to reach the swelling equilibrium. After the sample was removed, the surface was quickly dried with filter paper before weighing, and the mass m_2 was recorded. Five samples per group were measured, and the results were averaged.

3. Results

3.1. FT-IR

The silicone encapsulant used is a polymer with a silicon-oxygen bond (Si-O-Si) as the main chain. There are mainly four characteristic peaks in its FT-IR spectra, and the correspondence between the characteristic peaks and the characteristic groups is shown in Table 3. Figure 5 shows the spectra of the samples under different irradiation conditions. It is worth noting that the spectra before and after irradiation show that the wavenumber of characteristic peaks of silicone encapsulant had no change, indicating that no new groups were formed after irradiation. The absorbance of the characteristic peaks hardly changed, which indicates no change in the intensity of the characteristic peaks. Although the chemical reaction of silicone encapsulant occurred under irradiation, the change in characteristic groups was not detected by ATR-FITR. There are two possible reasons for this: ATR-FTIR is utilized to characterize the change in the surface groups of material and not to characterize the change in the material as a whole, and the pyroelectric sensor in ATR-FTIR is not sensitive enough to characterize changes in groups on the surface after irradiation. The change in the infrared spectrum of silicone encapsulant at the total radiation dose is consistent with that described in the references [20,21].

Table 3. Characteristic groups of silicone.

Wave Number/cm^{-1}	Characteristic Groups
2962	C-H
1257	Si-CH_3
1007	Si-O-Si
786	Si$(CH_3)_2$

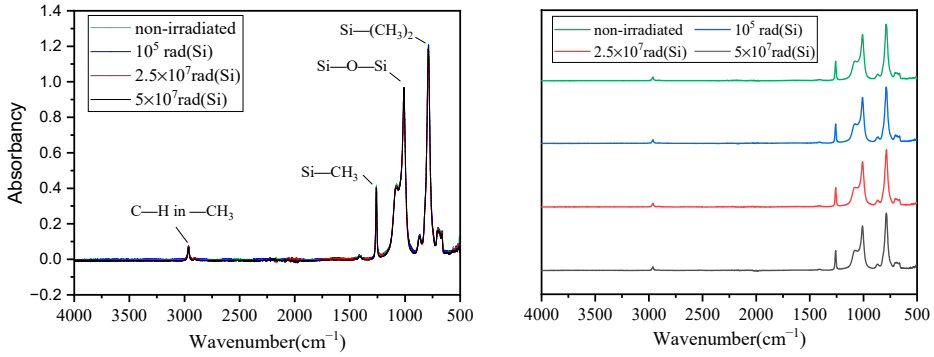

Figure 5. The spectra of the samples under different irradiation conditions. (**a**) Characteristic groups of silicone. (**b**) Comparison of infrared spectra of samples under different irradiation conditions.

3.2. SEM

Field emission SEM was used to observe the surface morphology of the silicone encapsulant. The results are shown in Figure 6. At 500× magnification, no significant differences are observed between the samples irradiated with 10^5 and 2.5 × 10^7 rad (Si) and the non-irradiated samples. Obvious cracks and pits can be seen on the surface of the sample irradiated with 5 × 10^7 rad (Si). Under irradiation, the silicone encapsulant had a crosslinking reaction, which caused the material to become harder and brittler gradually. When the irradiation dose reached a certain limit, the silicone encapsulant became over-crosslinked, hardening intensified, and microscopic cracks were generated. In addition, in the process of over-crosslinking, the pendant group of polymer molecules may have broken into small molecules, and small molecules volatilized to form pits.

3.3. Interface PD Inception Voltage

For high-voltage potting products, the PD magnitude was greater than 5PC, and the product was considered to be invalid. The voltage corresponding to a discharge magnitude of 5 PC was defined as the PD initiation voltage. Figure 7 shows the variation in the PD inception voltage with the irradiation dose. It can be seen from the figure that the PD inception voltage of the potting interface does not change significantly. The average value of the 10 valid data for each group of samples increases slightly with increasing irradiation dose.

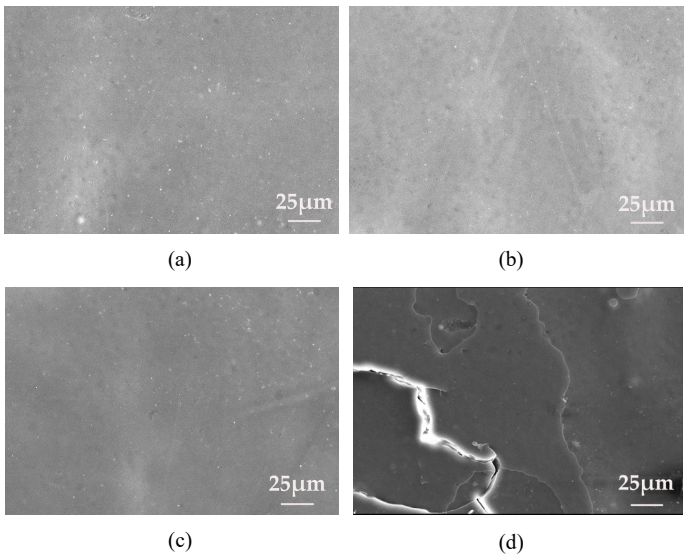

Figure 6. Microscopic morphology of different samples. (**a**) Non-irradiated, (**b**) 10^5 rad (Si), (**c**) 2.5 × 10^7 rad (Si), (**d**) 5 × 10^7 rad (Si).

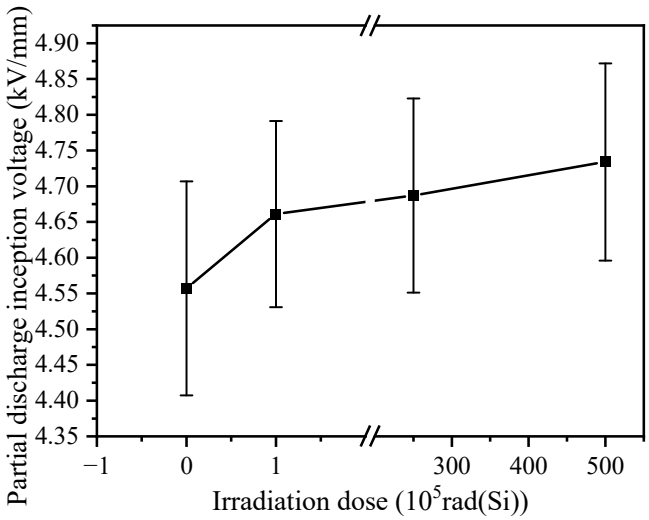

Figure 7. The variation of PD inception voltage with irradiation dose.

3.4. Interface Bonding

A 90° peel test was conducted on the samples before and after irradiation. Figure 8 shows the change in the peel strength with irradiation dose. The peel strength of the potting interface decreases with the increase in irradiation dose. However, all peel failures consist of cracking of the silicone encapsulant body, and the bonding interface is not delaminated. Polmanteer's theory and works by other researchers have explained the interfacial bonding mechanism using a solvent swelling method [33,34]. After soaking in toluene, only the dispersive adhesive layer detaches from the surface of the adhesive material, while the adhesive layer with hydrogen and chemical bonds does not detach. After soaking in an ammonia-saturated toluene solution, the adhesive layer with dispersion and hydrogen bonds detaches from the surface of the adhesive material, while the adhesive layer with the chemical bonds does not detach. The analysis results of the solution erosion and interface adhesion at the silicone encapsulant/FR-4 bonding interface are shown in Table 4.

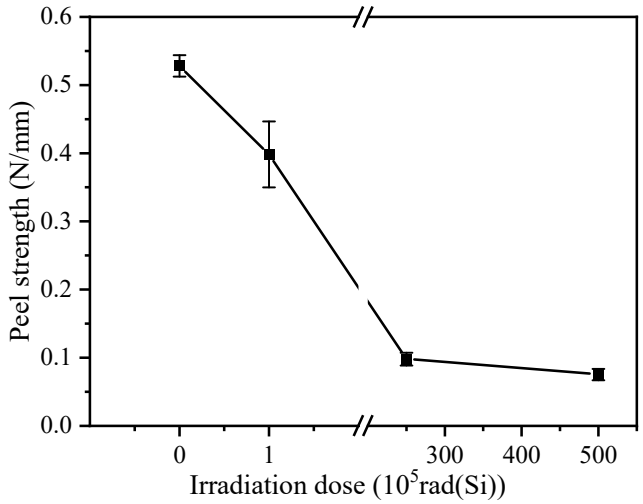

Figure 8. The change in peel strength with irradiation dose.

Table 4. Analysis of solution erosion and interface adhesion at silicone encapsulant/FR-4 bonding interface.

Irradiation Dose Rad (Si)	Fracture Forms		Interfacial Bonding		
	Toluene	Ammonia-Saturated Toluene Solution	Dispersion Bonding	Hydrogen Bond Interaction	Chemical Bonding
0	— [1]	—	+ [2]	(+) [3]	+
10^5	—	—	+	(+)	+
2.5×10^7	—	—	+	(+)	+
5×10^7	—	—	+	(+)	+

[1]: "—" in the table indicates that the silicone encapsulant did not fall off. [2]: "+" in the table indicates that there was such an interaction. [3]: "(+)" in the table indicates that there may have been such an interaction.

3.5. Physical Properties

3.5.1. Hardness

Figure 9 shows the trend of the hardness as a function of the irradiation dose. As can be seen in the figure, the hardness of the samples increases gradually with the increase in irradiation dose. The hardness of the non-irradiated silicone encapsulant is 32.9, while it is 50 for an irradiation dose of 5×10^7 rad (Si), which corresponds to a 76.3% increase. Hardness is an important parameter that influences the degree of softness of a polymer. The increase in hardness gradually causes the high elasticity of the silicone encapsulant to decrease, and this reduction in elasticity leads to an increase in the brittleness of the silicone encapsulant, increasing the internal stress, which may cause the fracture of components, such as chip resistors.

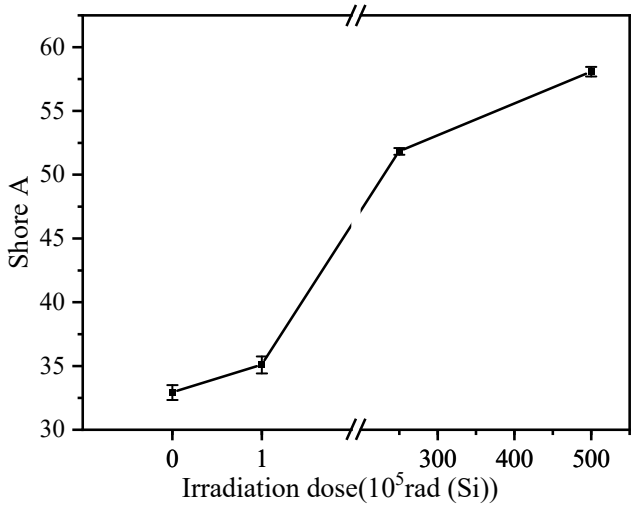

Figure 9. Changes in hardness under different irradiation conditions.

3.5.2. Mechanical Properties

The highly elastic state is characterized by the free movement of macromolecular chains and a high elasticity, which is unique to polymers. Polymers exhibit unique mechanical properties in the highly elastic state. The tensile strength, elongation at break, and elastic modulus can be used as characterization parameters to evaluate the elasticity of polymers. Figure 10a shows that the tensile strength of the silicone encapsulant first increases and then decreases with the increase in irradiation dose, reaching the maximum at 2.5×10^7 rad (Si). The elongation at break decreases with increasing irradiation dose; it is 56.3% for the specimens irradiated with a dose of 5×10^7 rad (Si), which is 83.8% lower than that of the non-irradiated specimens (348.6%). Figure 10b shows the change in elastic modulus. The elastic modulus of the sample irradiated with 5×10^7 rad (Si) is 2.65, while that of the non-irradiated sample is 0.68, which represents an increase of

289.7%.The gradual increase in the elastic modulus indicates that irradiation damaged the good compliance of the silicone encapsulant and caused the material to gradually harden.

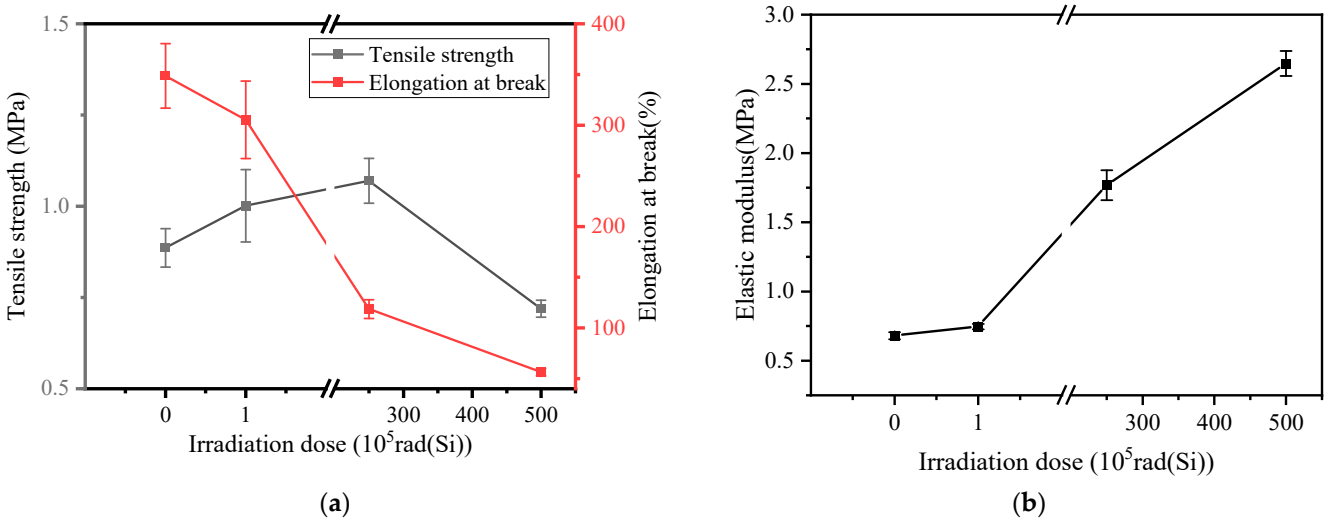

Figure 10. Changes in mechanical properties under different irradiation conditions. (**a**) Tensile strength and elongation at break. (**b**) Elastic modulus.

3.5.3. Thermal Behavior

1. Coefficient of thermal expansion

There is a great difference between the coefficient of thermal expansion of the silicone encapsulant, which is an elastomer, and that of the FR-4 plate, which is an epoxy glass fiber board. A good interfacial bonding can limit the difference in the thermal expansion behavior between the encapsulant and FR-4. However, changes in material elasticity and interfacial adhesion induced by irradiation can alter this limitation effect. Figure 11 shows the thermal expansion coefficient of the silicone encapsulant and potting interface as a function of temperature under different irradiation conditions. Since the interfacial shear force is more likely to cause interfacial debonding, thermal expansion in the shear direction was mainly tested.

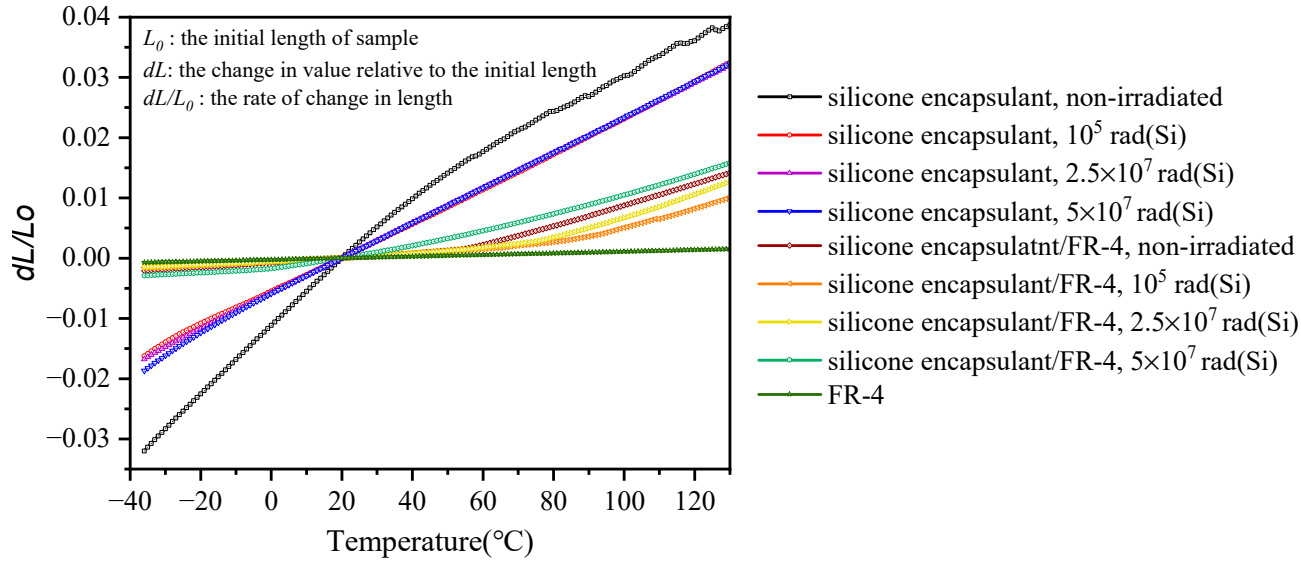

Figure 11. The thermal expansion deformation of silicone encapsulant and silicone encapsulant/FR-4.

As can be seen in Figure 11, the thermal expansion deformation of the potting interface is significantly smaller than that of the encapsulant. The irradiation reduces the thermal expansion deformation of the encapsulant, but there is little variation between different doses. The thermal expansion deformation of the potting interface above room temperature first decreases and then increases with the increase in irradiation dose. Taking 20 °C as the reference temperature, the coefficient of thermal expansion of the interface sample irradiated with 5×10^7 rad (Si) is 124.6×10^{-6} K^{-1}, while that of the non-irradiated sample is 93.9×10^{-6} K^{-1}, which represents an increase of 32.7%.

2. Dynamic mechanical properties

Figure 12 shows the change in the storage modulus (E′) of the silicone encapsulant under different irradiation doses. The storage modulus can provide information on the hardness of a material. With increasing irradiation dose, the storage modulus increases significantly. Furthermore, the storage modulus of the non-irradiated samples decreases as the temperature increases, while the storage modulus of the irradiated samples increases with the increase in temperature. The changes in the storage modulus of different irradiated samples at room temperature and the maximum operating temperature of 85 °C are shown in Table 5. At room temperature, the storage modulus of the sample irradiated with a dose of 5×10^7 rad (Si) increases by 335.9% compared with that of the non-irradiated sample, and at 85 °C, the percentage increase rises to 589.8%.

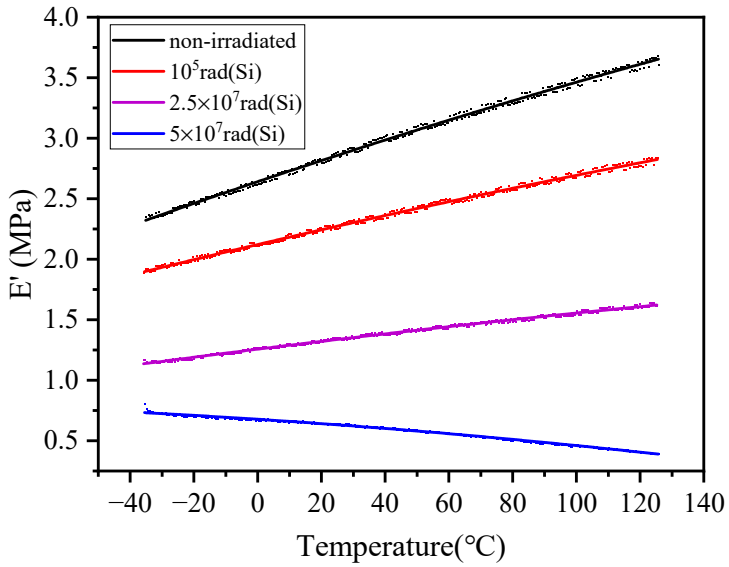

Figure 12. Changes in the storage modulus of Silicone encapsulant under different irradiation doses.

Table 5. Storage modulus of encapsulant with different radiation doses at different temperatures.

Samples	E′(MPa)		Percentage Increase Relative to Non-Irradiated (%)	
	20 °C	85 °C	20 °C	85 °C
Non-irradiated	0.64	0.49	0	0
10^5	1.31	1.49	104.7	204.1
2.5×10^7	2.22	2.60	246.9	430.6
5×10^7	2.79	3.38	335.9	589.8

3.6. Electrical Properties

3.6.1. Dielectric Constant and Dielectric Loss Factor

Figure 13 shows the variation in the dielectric constant and dielectric loss factor for samples at different irradiation doses at different frequencies. The dielectric constant and

dielectric loss factor were measured at four frequency points, and both of them were found to decrease with the increase in frequency. The difference between the two is that the dielectric constant increases with the increase in irradiation dose, while the dielectric loss factor decreases with the increase in irradiation dose. The data at 1 MHz are taken as an example. The dielectric constant is 2.72 for the specimens irradiated with a dose of 5×10^7 rad (Si), which is 5.0% higher than that of the non-irradiated specimens (2.59). The dielectric loss factor of the sample irradiated with 5×10^7 rad (Si) is 0.0035, while that of the non-irradiated sample is 0.0083, which represents a decrease of 57.8%.

3.6.2. Volume Resistivity

Volume resistivity, which is the impedance of a material to current per unit volume, is used to characterize the electrical properties of a material. Figure 14 shows the change in the volume resistivity under different irradiation conditions; it can be seen that the volume resistivity increases with the increase in irradiation dose, but its order of magnitude does not change. The volume resistance is on the order of 10^{14} $\omega\cdot$ cm. The volume resistivity of the non-irradiated silicone encapsulant is 1.27×10^{14} $\omega\cdot$ cm, while it is 6.30×10^{14} $\omega\cdot$cm for an irradiation dose of 5×10^7 rad (Si), which corresponds to a 396.1% increase.

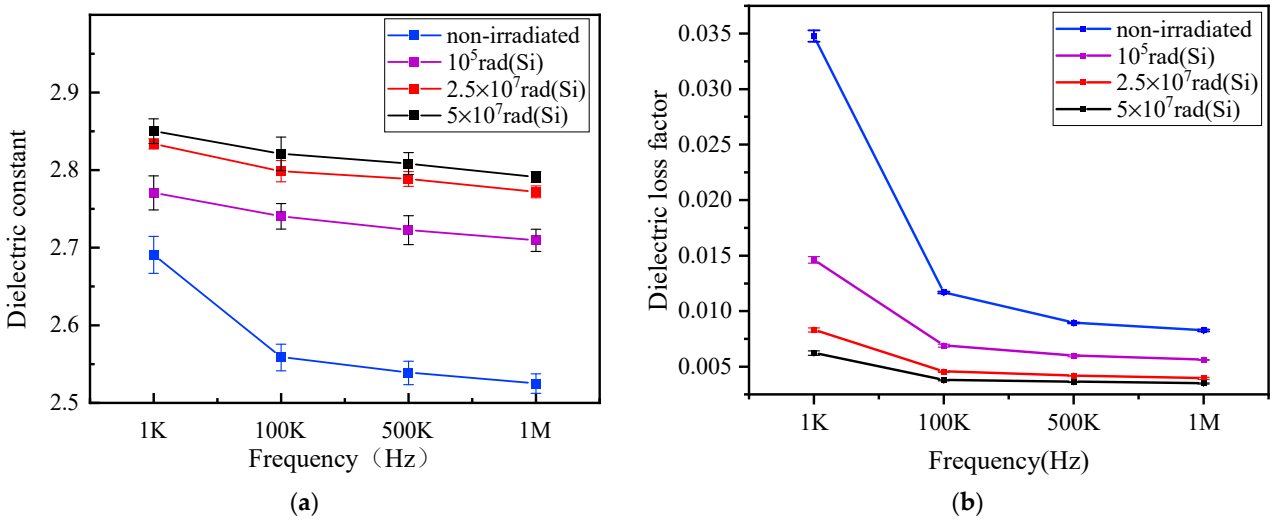

Figure 13. Variation in dielectric constant and dielectric loss factor for samples with different irradiation doses at different frequencies. (**a**) Dielectric constant, (**b**) Dielectric loss factor.

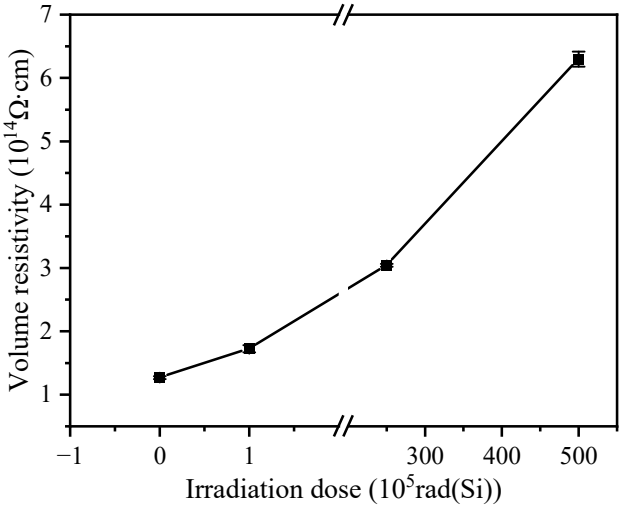

Figure 14. Volume resistivity.

3.6.3. Breakdown Strength

A two-dimensional Weibull distribution was used for statistical analysis. The cumulative breakdown probability is 63.2% [7], and the corresponding specimen breakdown strength determines the average breakdown strength of a material. Figure 15 shows the breakdown strength of the Weibull distribution. E_b represents the breakdown strength corresponding to a 63.2% probability of failure. The slope of the Weibull distribution reflects the dispersion of the data. With increasing irradiation dose, the breakdown strength is first increasing and then decreasing. The breakdown strength is 22.6 kV/mm for the specimens irradiated with a dose of 5×10^7 rad (Si), which is 9.5% lower than that of the non-irradiated specimens (24.98 kV/mm).

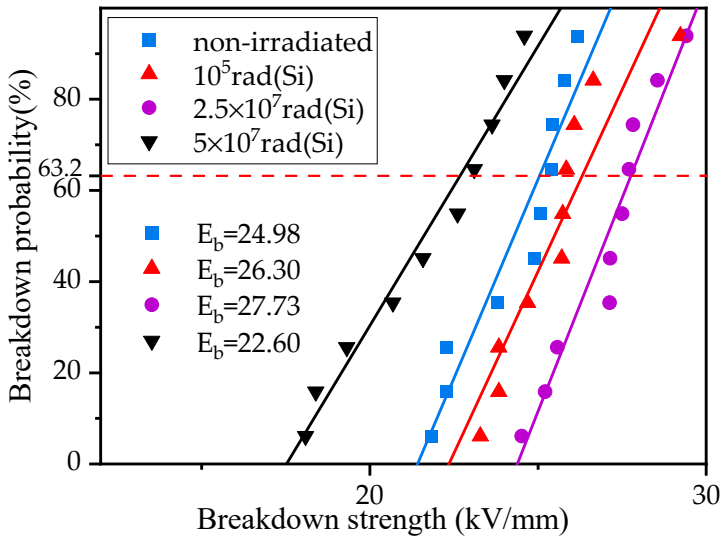

Figure 15. Breakdown strength.

4. Discussion

4.1. Analysis of the Effects of Irradiation on the Properties of Silicone Encapsulant

Under irradiation, atoms and/or molecules in the material are ionized and/or excited, forming ions, electrons, and excited atoms or molecules. The excited molecule dissociates into free radicals. Finally, reactions such as crosslinking or cracking occur between the free radicals and the molecules or free radicals themselves, resulting in changes in the chemical structure of the material, thereby causing changes to the material properties [7]. The variation in the properties can be analyzed in terms of the variation in the material crosslinking density [35]. The crosslinking density of the silicone encapsulant was calculated using the equilibrium swelling method [36,37].

$$\varphi = \frac{m_1/\rho_1}{m_1/\rho_1 + (m_2 - m_1)/\rho_c} \quad (1)$$

$$M_c = \frac{\rho_1 V_0 \varphi^{\frac{1}{3}}}{\ln(1-\varphi) + \varphi + \chi\varphi^2} \quad (2)$$

$$D = \frac{1}{2M_c} \quad (3)$$

where m_1 is the mass of the silicone encapsulant before swelling, ρ_1 is the density of the silicone encapsulant before swelling, m_2 is the mass of the silicone encapsulant when it reaches swelling equilibrium, ρ_c is the density of toluene, φ is the volume fraction of the silicone encapsulant in the swelling solvent, M_c is the average molecular weight of the effective chain between two adjacent crosslinking points, V_0 is the molar volume of toluene (107 mL/mol), χ = 0.456 is a constant that characterizes the interaction between the silicone encapsulant and toluene, and D is the crosslinking density of the silicone encapsulant.

Figure 16 shows the variation trend in the crosslinking density of the silicone encapsulant before and after irradiation. It can be seen that with the increase in irradiation dose, the crosslinking density of the silicone rubber increases. This shows that the silicone encapsulant is mainly irradiated crosslinking. The crosslinking density is 27.03 $\times$ 10^{-5} mol/g for the specimens irradiated with a dose of 5 $\times$ 10^{7} rad (Si), which is 301.6% higher than that of the non-irradiated specimens (6.73 $\times$ 10^{-5} mol/g).

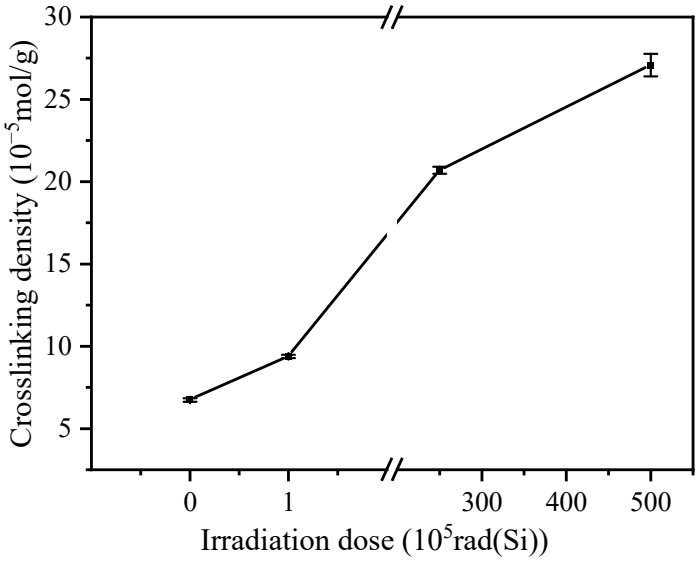

Figure 16. Crosslinking density.

The hardness and the elongation at break depend on the flexibility of the polymer chain, and the hardness increases with the reduction of the flexibility of the polymer chain, while the elongation at break shows the opposite law. Due to the crosslinking reaction of the silicone encapsulant under irradiation, a denser network structure is formed. This structure inhibits slipping between the polymer chains and reduces the compliance of the polymer, resulting in a lower elongation at break and an increased hardness. The tensile strength first increases and then decreases with the increase in irradiation dose. This is because crosslinking plays a leading role at the beginning, and the material strength is enhanced when the irradiation reaches a certain threshold, after which the material strength begins to decrease due to excessive cross-linking.

Being a polymer, the volume resistivity of the silicone encapsulant mainly depends on its internal carrier concentration and carrier mobility. Intrinsic ions are typically absent in organic dielectrics, and conductive carriers originate from impurities, including small amounts of monomers and various additives that do not participate in the reaction during synthesis. Furthermore, the carrier mobility is related to the size of the free volume inside the polymer. The irradiation increases the crosslinking of the silicone encapsulant, resulting in a denser internal network structure of the material, a decrease in the carrier concentration, and a smaller free volume, thereby changing the charge migration within t the material so that the volume resistivity of the silicone rubber after irradiation increases slightly.

When subjected to irradiation, the silicone encapsulant produces many free radicals, ions, electrons, and other active particles, resulting in complex chemical reactions. When high-energy radiation acts on the side chains or side groups of a macromolecule, the $H^{\bullet}$, which is produced after the dissociation of the chemical bonds, takes an $H^{\bullet}$ from a neighboring molecule to generate H_2, or the side groups break into low-molecular free radicals, which are easily polarized under the action of the electric field. Thus, the relative dielectric constant of the silicone encapsulant increases slightly with the increase in irradiation dose.

Under an alternating electric field, the dielectric signal of the silicone encapsulant is mainly contributed to by the conductivity loss. Due to the volatilization of the residual cross-linked byproducts in the silicone rubber after irradiation and further cross-linking between the subsequent molecular chains, the diffusion and migration of the internal charges in the medium are hindered, and the conductivity loss gradually decreases. Therefore, the dielectric loss factor gradually decreases, corresponding to the result of volume resistivity [38].

According to the free volume breakdown theory, the length of the free volume determines the mean free path, which in turn determines the breakdown strength. The reduction in the free volume causes the carrier to obtain less energy in the free path, which is not enough to cross the threshold barrier corresponding to the breakdown, and thus the breakdown strength is increased. However, as the irradiation dose continues to increase, the silicone rubber is over-crosslinked, hardening intensifies and microscopic cracks are generated so that the breakdown strength is reduced.

4.2. Thermal Behavior Analysis of the Silicone Encapsulant after Irradiation

The DMA and thermal expansion deformation behavior analysis are both thermal analysis methods that can be used to study the variation in the viscoelastic properties and expansion behavior of materials with temperature; furthermore, they are of great significance for analyzing the thermal stress inside the material [39].

The glass transition temperature of the silicone encapsulant is −119 °C, and the silicone encapsulant is rubber in the temperature range of −35–125 °C. With the increase in temperature, the molecules become free to move, and the storage modulus is gradually reduced. However, the storage modulus after irradiation changes significantly with temperature. The storage modulus of the irradiated silicone encapsulant gradually increased with increasing temperature. This is possibly because as the temperature rises, the thermal effects accumulated inside the material trigger a post-curing of the resin, which in turn hinders the movement of the intermolecular chain segments. The molecular chains are limited by an increased number of cross-linking points and their flexibility is reduced, so the storage modulus increases. The flexibility of the molecular chains is reduced due to the restriction imposed by the increased number of crosslinking points, so the storage modulus increases accordingly.

The silicone encapsulant is a polymer, and its thermal expansion behavior consists of thermal expansion and cold contraction. The thermal deformation of the encapsulant before and after irradiation gradually increases with the increase in temperature, but the thermal deformation of the irradiated silicone rubber is smaller than that of the non-irradiated silicone encapsulant. This is because irradiation causes the crosslinking density of the silicone rubber to increase, and the increase in crosslinking density hinders the movement of the polymer segments. However, regarding the interfacial thermal expansion, due to the combined influence of the interface bonding strength and the crosslinking density of the silicone encapsulant, the thermal expansion deformation first decreases and then increases. When the decrease in thermal expansion deformation caused by the increase in crosslinking density is greater than the increase in thermal expansion deformation caused by the decrease in interfacial bonding strength, the interfacial thermal expansion deformation decreases, and vice versa.

Overall, the combined effects of irradiation and heat made the encapsulant harder and more brittle, and the interface bonding strength gradually decreased. Irradiation coupled with thermal stress can induce material cracking and interface debonding.

4.3. Analysis of the Interfacial PD

For high-voltage potted modules, potting interface breakdown, which is usually caused by deterioration of the interface PD, is the main form of insulation failure. The continuous PD causes the discharge channel to extend until insulation breakdown occurs [3]. The interface PD is closely related to the interface state. From a microscopic point of

view, the interface can be considered as being composed of irregular contact surfaces and micropores. According to the Paschen law [40], the discharge inception field (E_v) of voids is related to the pressure (P) and size (d) of gas:

$$E_v = (P_0/P)\frac{A}{d^2} + (P/P_0)B + \frac{C}{d} + (P/P_0)^{0.5}\frac{D}{d^{0.5}} \quad (4)$$

where P_0 = 1 atm; A = 0.00101 kV·mm, B = 2.4 kV/mm, C = −0.0097 kV, D = 2.244 kV·mm$^{-0.5}$.

At constant interfacial pressure, the gas discharge initiation field is related to the size of the voids. The larger the voids, the lower the PD inception field. Interestingly, although the interfacial peel strength gradually decreases with the increase in irradiation dose, the PD inception voltage does not decrease with the decrease in peel strength. In the actual PD inception voltage test, the average value of the PD inception voltage increases slightly with the increase in irradiation dose.

Considering that the magnitude of the local electric field intensity affects the PD inception voltage, we used computer simulation technology (CST) to simulate the electric field intensity distribution of the needle-plate electrode. The CST static electric field solver was used for the simulation, using a tetrahedral mesh with a 0.0001 mm mesh cell edge. Figure 17 shows the simulation modeling of the needle-plate electrode. Figure 18 shows the simulation results of the electrostatic field intensity of the needle-plate electrodes of the potting materials with different dielectric constants. The results show that a greater dielectric constant leads to a lower electric field strength.

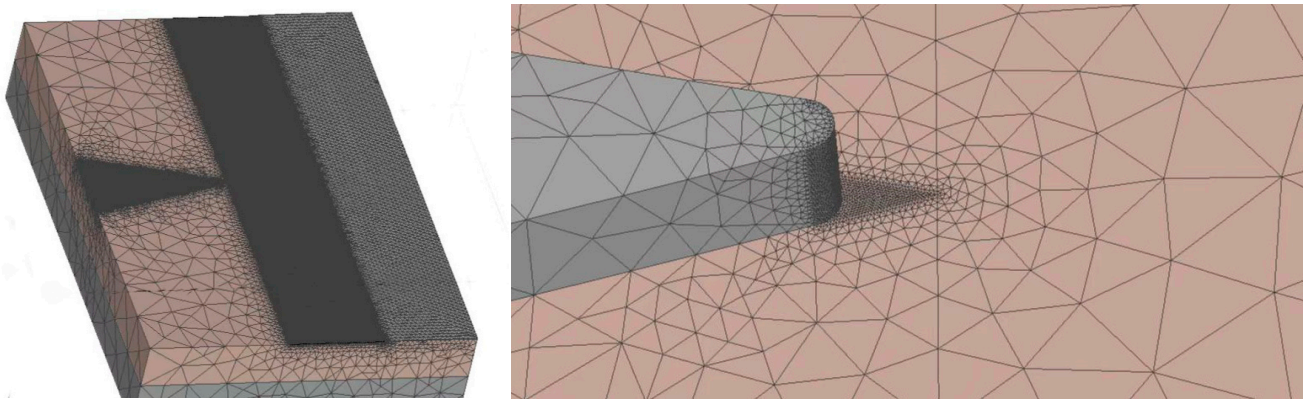

(a) (b)

Figure 17. Simulation modeling of the needle-plate electrode. (**a**) The modeling of the needle-plate electrode. (**b**) A local zoomed view of the needle.

In conclusion, there may be two reasons for the observed increase in the PD inception voltage. Firstly, after irradiation, although the peel strength of the potting interface is reduced, no interface delamination occurs, and the interface is still bonded via chemical bonds. The status of the potting interface does not change. Secondly, the dielectric constant of the material increases slightly, resulting in a slight decrease in the local electric field strength of the needle electrode, which increases the PD inception voltage.

Meanwhile, we prepared bonding defect samples for PD testing. The maximum PD inception voltage of the defective samples did not exceed 2.56 kV. This indicates that the PD inception voltage is closely related to the interface bonding state.

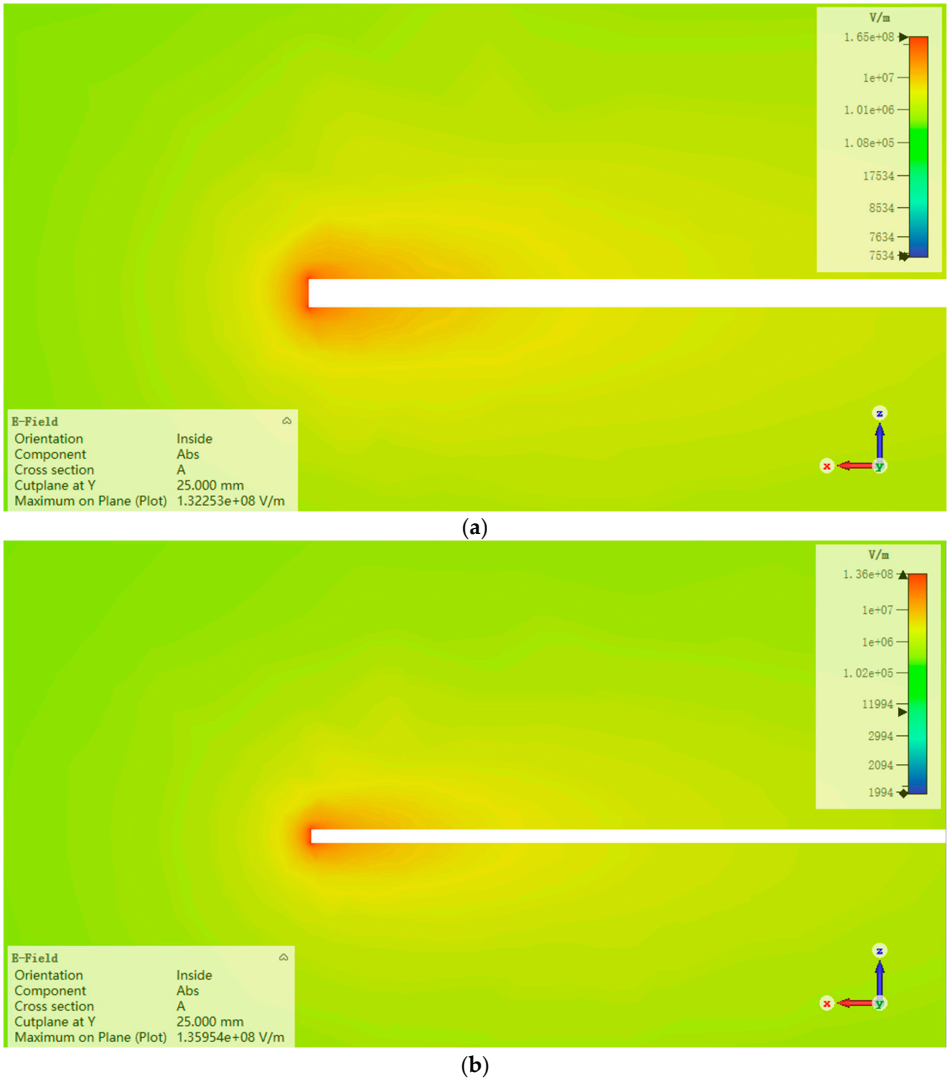

Figure 18. Simulation results of the electrostatic field intensity of the needle-plate electrodes. (**a**) The dielectric constant is 2.72; (**b**) the dielectric constant is 2.59.

5. Conclusions

A comprehensive evaluation method was designed to evaluate the potted module based on silicone encapsulant. This method evaluates the physical and electrical properties of the encapsulant as well as the encapsulated interface properties.

(1) With γ-radiation, the variations of physical properties, electrical properties, and encapsulated interface properties were measured. The results are as follows:
(2) The silicone encapsulant mainly experienced irradiation crosslinking; with the increase in irradiation dose, the silicone encapsulant gradually became harder and more brittle. It demonstrated an increased crosslinking density, hardness, elastic modulus, volume resistivity, and dielectric constant with increasing irradiation dose as well as a decreased elongation at break and dielectric loss factor. The tensile strength and the breakdown strength show the same trend with increasing irradiation dose, both first increasing and then decreasing. At a dose of 5×10^7 rad (Si), the irradiation aging of the silicone encapsulant is pronounced, and the potted modules subjected to this irradiation dose need to be reinforced, or the encapsulant needs to be modified.
(3) The thermal behavior analysis of the encapsulant after irradiation shows that the combined effects of irradiation and heat aggravated the deterioration of the encapsulant. At room temperature, the storage modulus of the sample irradiated with a dose of

5×10^7 rad (Si) increased by 335.9% compared with that of the non-irradiated sample, and at 85 °C, the percentage increase rose to 589.8%. Taking 20 °C as the reference temperature, the coefficient of thermal expansion of the interface sample irradiated with a dose of 5×10^7 rad (Si) was 124.6×10^{-6} K^{-1}, while that of the non-irradiated sample was 93.9×10^{-6} K^{-1}, i.e., an increase of 32.7%.

(4) Irradiation reduced the peel strength of the potting interface but does not cause the breaking of the interfacial chemical bonds. The CST simulation shows that the highest electric field intensity of the interface is related to the dielectric constant, and the increase in the dielectric constant reduces the electric field intensity. The interface PD inception voltage increases slightly with increasing irradiation dose. However, the inception voltage of the PD of the interfacial defective samples is much lower than that of well-bonded samples, indicating that the interfacial PD is closely related to the bonding state.

(5) The advantage of the applied method is that the property changes of samples can be comprehensively evaluated, while the weaknesses are that much test equipment, a large sample size, and many test variables are needed.

(6) In this work, we only investigated the interface between FR-4 and encapsulant. In fact, there are a variety of interfaces, such as ceramic–encapsulant interface and epoxy–encapsulant interface in electronic components on high-voltage printed circuit boards, that should be further studied in the future work.

Author Contributions: Conceptualization, C.H. and G.W.; methodology, C.H., G.W., Y.F. and B.Z.; validation, C.H., W.Z. and B.Z.; formal analysis, C.H.; investigation, C.H. and Y.F.; resources, C.H. and W.Z.; data curation, C.H. and W.Z.; writing—original draft preparation, C.H.; writing—review and editing, B.Z., G.W., Y.F., H.L. and K.Z.; visualization, W.Z.; supervision, C.H.; project administration, C.H.; funding acquisition, C.H. All authors have read and agreed to the published version of the manuscript.

Funding: This paper is a part of the project named Application of High Efficiency Partial Power Regulation on Space Travelling-wave Tube Amplifiers (No. 62201546), which is sponsored by National Natural Science Foundation of China.

Data Availability Statement: Not applicable.

Conflicts of Interest: The authors declare no conflict of interest.

Nomenclature

STWTA	Space traveling-wave tube amplifier
EPC	Electronic power conditioner
CTE	Coefficient of thermal expansion
DMA	Dynamic mechanical analysis
TMA	Thermomechanical analysis
PD	Partial discharge
FT-IR	Fourier transform infrared spectroscopy
ATR-FTIR	Attenuated total reflection Fourier transform infrared spectroscopy
SEM	Scanning electron microscope
CTS	Computer simulation technology

References

1. Li, Z.-C. The current status and developmental trends of space travelling wave tube amplifier. *Space Electron. Technol.* **2012**, *4*, 28–34.
2. Pequet, E.; Delporte, P.; Fayt, P.; Gak, M.; Canon, T. ESA qualified EPC for telecommunication satellites TWTA. In Proceedings of the Abstracts. International Vacuum Electronics Conference 2000 (Cat. No. 00EX392), Monterey, CA, USA, 2–4 May 2000; pp. 1–2.
3. Secretariat, E.C.S.S. *Space Engineering High-Voltage Engineering and Design Handbook*; ESA Special Publication: Noordwijk, The Netherlands, 2014; p. 133.
4. Ardebili, H.; Zhang, J.; Pecht, M.G. *Encapsulation Technologies for Electronic Applications*; William Andrew: Norwich, NY, USA, 2018.

5. Boudjemai, A.; Hocine, R.; Guerionne, S. Space environment effect on earth observation satellite instruments. In Proceedings of the 2015 7th International Conference on Recent Advances in Space Technologies (RAST), Istanbul, Turkey, 16–19 June 2015; pp. 627–634.
6. Chen, J.; Ding, N.; Li, Z.; Wang, W. Organic polymer materials in the space environment. *Prog. Aerosp. Sci.* **2016**, *83*, 37–56. [CrossRef]
7. Wang, J.-H.; Zhong, L.-S. *Handbook of Electrical Electronic Insulation Technology*; China Machine Press: Beijing, China, 2008.
8. Palsule, A.S.; Clarson, S.J.; Widenhouse, C.W. Gamma irradiation of silicones. *J. Inorg. Organomet. Polym. Mater.* **2008**, *18*, 207–221. [CrossRef]
9. Chen, H.-B.; Qin, Z.-M.; Wang, P.-D.; Liu, B.; Huang, W. Recent progress in irradiation-induced aging of silicones. *J. Radiat. Res. Radiat. Process.* **2020**, *38*, 3–11.
10. Hanisch, F.; Maier, P.; Okada, S.; Schönbacher, H. Effects of radiation types and dose rates on selected cable-insulating materials. *Int. J. Radiat. Appl. Instrum. Part C. Radiat. Phys. Chem.* **1987**, *30*, 1–9. [CrossRef]
11. Clavreul, R. Effects of thermal and radiation stresses on elastomer properties. In Proceedings of the IEEE 1997 Annual Report Conference on Electrical Insulation and Dielectric Phenomena, Minneapolis, MN, USA, 19–22 October 1997; Volume 2, pp. 414–417.
12. Pinel, B.; Boutaud, F. A methodology to predict the life duration of polymers used in nuclear power stations. Industrial needs and their approach. *Nucl. Instrum. Methods Phys. Res. Sect. B Beam Interact. Mater. At.* **1999**, *151*, 471–476. [CrossRef]
13. Ohki, Y.; Hanada, S.; Miyamoto, M.; Hirai, N.; Yang, L. Aging mechanism of silicone rubber by heat and gamma-rays. In Proceedings of the 2016 IEEE Conference on Electrical Insulation and Dielectric Phenomena (CEIDP), Toronto, ON, Canada, 16–19 October 2016; pp. 869–872.
14. Maxwella, R.S.; Cohenourb, R.; Sungb, W.; Solyomb, D. The effects of g-radiation on the thermal, mechanical, and segmental dynamics of a silica filled, room temperature vulcanized polysiloxane rubber. *Polym. Degrad. Stab.* **2003**, *80*, 443–450. [CrossRef]
15. Rajini, V.; Udayakumar, K. Degradation of silicone rubber under AC or DC voltages in radiation environment. *IEEE Trans. Dielectr. Electr. Insul.* **2009**, *16*, 834–841. [CrossRef]
16. Ito, S.; Hirai, N.; Ohki, Y. Changes in mechanical and dielectric properties of silicone rubber induced by severe aging. *IEEE Trans. Dielectr. Electr. Insul.* **2020**, *27*, 722–730. [CrossRef]
17. Jing, P.; Zhi, L.; Peng, W.; Qian, J.; Chun, J.-W.; Yu, X.-L. Research on Ultraviolet Aging Properties of Modified Silicone Rubber for Composite Insulator. In Proceedings of the 2020 International Symposium on Electrical Insulating Materials (ISEIM), Tokyo, Japan, 13–17 September 2020; pp. 202–205.
18. Traeger, R.K.; Castonguay, T.T. Effect of γ-radiation on the dynamic mechanical properties of silicone rubbers. *J. Appl. Polym. Sci.* **1966**, *10*, 535–550. [CrossRef]
19. Guo, R.; Li, D.-T.; Yang, S.-S.; Feng, Z.-Z.; Huang, Y.-F.; Zhao, C.-X. Study on failure mechanism of silicone rubber GD414 induced by gamma irradiation. *Vac. Cryog.* **2015**, *21*, 222–226. [CrossRef]
20. He, D.-P.; Yuan, C.-P.; Wang, N.; Zhang, J.-J.; Gao, H.; Xing, Y. Applicability of vulcanized silicone rubber used in encapsulation of aerospace device. *J. Nanjing Univ. Aeronaut. Astronaut.* **2019**, *51*, 118–124.
21. Liu, B.; Liu, Q.; Ao, Y.; Wang, P.; Huang, W.; Chen, H. Gamma irradiation-induced degradation of silicone encapsulation. *Mater. Today Commun.* **2022**, *31*, 103476. [CrossRef]
22. Ebke, T.; Khaddour, A.; Peier, D. Degradation of silicone gel by partial discharges due to different defects. In Proceedings of the 2000 Eighth International Conference on Dielectric Materials, Measurements and Applications (IEE Conf. Publ. No. 473), Edinburgh, UK, 17–21 September 2000; pp. 202–207.
23. Sato, M.; Kumada, A.; Hidaka, K.; Yamashiro, K.; Hayase, Y.; Takano, T. Degradation process of silicone-gel by internal surface discharges. In Proceedings of the 2014 IEEE 18th International Conference on Dielectric Liquids (ICDL), Bled, Slovenia, 29 June 2014–3 July 2014; pp. 1–4.
24. Sato, M.; Kumada, A.; Hidaka, K.; Yamashiro, K.; Hayase, Y.; Takano, T. Surface discharges in silicone gel on AlN substrate. *IEEE Trans. Dielectr. Electr. Insul.* **2016**, *23*, 494–500. [CrossRef]
25. Sato, M.; Kumada, A.; Hidaka, K.; Yamashiro, K.; Hayase, Y.; Takano, T. Dynamic potential distributions of surface discharge in silicone gel. *IEEE Trans. Dielectr. Electr. Insul.* **2015**, *22*, 1733–1738. [CrossRef]
26. Yang, Z.; Li, K.; Jiang, X.; Zhang, B.; Li, X. The Degradation Behaviors from Triple Junctions in IGBT Power Modules. In Proceedings of the 2022 IEEE International Conference on High Voltage Engineering and Applications (ICHVE), Chongqing, China, 25–29 September 2022; pp. 1–5.
27. Pieterse, P.J.; Bekker, M.; Arumugam, S.; Uhrlandt, D. Breakdown of Water Saturated Printed Circuit Boards in Dielectric Encapsulation for Deep-Sea Applications. In Proceedings of the 2022 IEEE Conference on Electrical Insulation and Dielectric Phenomena (CEIDP), Denver, CO, USA, 30 October–2 November 2022; pp. 393–396.
28. Kulkarni, R.; Soltani, M.; Wappler, P.; Guenther, T.; Fritz, K.P.; Groezinger, T.; Zimmermann, A. Reliability study of electronic components on board-level packages encapsulated by thermoset injection molding. *J. Manuf. Mater. Process.* **2020**, *4*, 26. [CrossRef]
29. Jalar, A.; Zain, S.M.M.S.M.; Ani, F.C.; Ramli, M.R.; Abu Bakar, M. Effect of potting encapsulation on crack formation and propagation in electronic package. In Advances in Robotics. In *Automation and Data Analytics: Selected Papers from iCITES 2020*; Springer International Publishing: Cham, Switzerland, 2020; pp. 351–357.
30. Chen, L.-Y.; Gao, Y.; Wang, X.-Y.; Huang, S.-H.; Du, B.-X. Analysis of Breakdown Process at the Interface Between Polypropylene and Silicone. *Proc. CSU-EPSA* **2018**, *30*, 8–12.

31. Wagner, M. *Thermal Analysis in Practice: Fundamental Aspects*; Carl Hanser Verlag GmbH Co KG: Munich, Germany, 2017.
32. Hasheminezhad, M.; Ildstad, E. Application of contact analysis on evaluation of breakdown strength and PD inception field strength of solid-solid interfaces. *IEEE Trans. Dielectr. Electr. Insul.* **2012**, *19*, 1–7. [CrossRef]
33. Polmanteer, K.E.; Lentz, C.W. Reinforcement studies—Effect of silica structure on properties and crosslink density. *Rubber Chem. Technol.* **1975**, *48*, 795–809. [CrossRef]
34. Botter, W.; Ferreira Soares, R.; Galembeck, F. Interfacial reactions and self-adhesion of polydimethylsiloxanes. *J. Adhes. Sci. Technol.* **1992**, *6*, 791–805. [CrossRef]
35. Charlesby, A.; Morris, J.; Montague, P. Mechanisms of reinforcement of silicone rubbers crosslinked by radiation. In *Journal of Polymer Science Part C: Polymer Symposia*; Wiley Subscription Services, Inc., A Wiley Company: New York, NY, USA, 1967; Volume 16, pp. 4505–4513.
36. Wang, Z.-L. Crosslinking density and determination method of rubber. *World Rubber Ind.* **1998**, *25*, 41–46, 35.
37. Zhou, Y.-X.; Zhang, Z.-H.; Zhang, Y.-X.; Zhu, X.-Q.; Huang, M. The Effect of Combined Thermal-Mechanical Aging on the Cross-Linking Network and Mechanical and Electrical Properties of Silicone Rubber. *Trans. China Electrotech. Soc.* **2022**, *37*, 4474–4486.
38. Wang, N.-C.; He, Y.-Y.; Kang, H.-W.; Wang, Z.; Jin, H.-Y. Thermal Aging and Ultrasonic Characteristics of Silicone Rubber for Cable Joint Insulation. *High Volt. Eng.* **2021**, *49*, 3181–3188.
39. Chen, Z.; Zhang, Q.; Wang, K.; Chen, M.; Liu, S. Fluid–solid coupling thermo-mechanical analysis of high power LED package during thermal shock testing. *Microelectron. Reliab.* **2012**, *52*, 1726–1734. [CrossRef]
40. Dissado, L.A.; Fothergill, J.C. *Electrical Degradation and Breakdown in Polymers*; IET: Hertfordshire, UK, 1992; Volume 9.